World Journal of Engineering Research
Print ISSN: 2959-9865
Online ISSN: 2959-9873
DOI: https://doi.org/10.61784/wjer3085

WINCH-BASED AND CABLE-DRIVEN JOINT ACTUATOR WITH TWO-STAGE REDUCTION MECHANISM

RongChuan Huang, LiJun Zhu*
School of Artificial Intelligence and Automation, Huazhong University of Science and Technology, Wuhan 430074, Hubei, China.
**Corresponding Author: LiJun Zhu*

Abstract: This paper presents a compact winch-based, cable-driven joint actuator with a two-stage reduction mechanism aimed at improving weight, backdrivability, and impact tolerance of robotic joints within constrained volumes. The design integrates primary and secondary reduction stages with an optimized winding scheme and an in-situ tensioning mechanism for stable transmission. A practical dual-encoder scheme provides an absolute output angle after power cycling. We detail the mechanical structure, winding/tensioning strategy, and electronics, and report measurements of reduction ratio, required pre-tension, and output stiffness. Experiments show a highly effective reduction ratio and predictable output stiffness consistent with modeling, with improved backdrivability under comparable size and mass. The module is suitable for compact legged/humanoid systems.
Keywords: Cable-driven actuator; Two-stage reduction; Winch-based reducer; Joint design

1 INTRODUCTION

Recent years have seen various joint designs and transmission methods for legged robots. Mainstream solutions like gear-driven reducers (e.g., MIT's quadruped[1]) and planetary roller screws (e.g., Tesla's humanoid[2]) offer high stiffness and precision but are often heavy, exhibit poor backdrivability at high ratios, and have low impact tolerance due to rigidity.
Cable-driven transmissions present a compelling alternative, reducing weight, improving backdrivability, and providing compliance for better impact resistance. Most cable-driven systems use remote actuation, moving motors to the torso to lower distal inertia, but this leads to long transmission paths and large volumes. Winch-based reducers, like in the Stanley project[3], improve backdrivability and flexibility, yet their bulky joints hinder use in compact spaces.

1.1 Related Work

Research in joint actuation includes compliant actuators, cable-driven reducers, and cable transmission systems. Negrello et al.'s Modular Compliant Actuator integrates elastic elements for adjustable stiffness, enhancing impact absorption[4]. The Stanley project's winch-based reducer improves joint backdrivability but has a large form factor[3]. Cable transmission systems, such as the low-inertia LIMS2-AMBIDEX[5] and OMRON's fully orthogonal robotic arm[6], achieve high speed. Additionally, some cable-driven trunk-like robots have attained high precision[7-8]. While existing methods excel individually in stiffness adjustment, backdrivability, or compactness, achieving a joint design that simultaneously offers a high reduction ratio, low backdrivability, impact resistance, and high precision within a constrained space remains a key challenge[6].

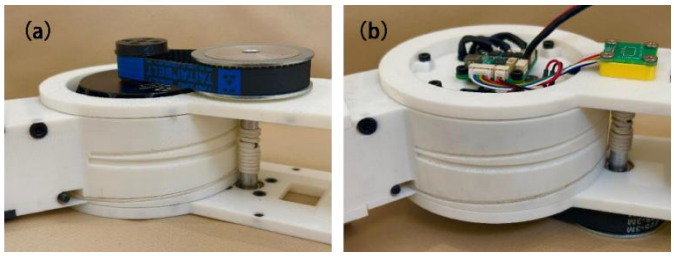

Figure 1 Winch-Based, Cable-Driven Joint Actuator with Two-Stage Reduction

1.2 Contributions

This paper presents a compact, two-stage winch-based cable-driven joint actuator (Figure 1) to address the above challenges. The design integrates primary and secondary winch reduction stages. An optimized cable winding scheme enhances transmission efficiency, while a built-in tensioning mechanism enables cable tension measurement and adjustment in confined spaces, improving stability. This system provides the absolute output shaft position upon startup, increasing control accuracy and operational reliability.

© By the Author(s) 2026, under the CC BY-NC-ND license (http://creativecommons.org/licenses/by-nc-nd/4.0).

The remainder of this paper is organized as follows: Section II describes the mechanical structure and dimensional design of the joint module. Section III discusses the cable winding and tensioning methods in detail, along with experimental evaluations of friction and tension. Section IV introduces the circuit design and implementation of the dual-encoder system. Finally, Section V presents experimental analyses and concludes the paper, respectively.

2 STRUCTURE INTRODUCTION

This section mainly introduces the specific structure of the winch-based and cable-driven joint actuator, along with the design methods considering its reduction ratio and dimensions.

2.1 Four Structural Configurations

Two possible motor mounting methods and two types of reduction mechanisms result in four distinct structural configurations.

2.1.1 Choices for motor mounting methods

External Fixed Structure: As shown in Figure 2(a), the motor is fixed to the transmission side plate. The circuit and transmission plates are stationary, while the winch winding wheel rotates relative to them via a tapered roller bearing. This arrangement suits applications where the transmission plate is fixed, avoiding rotation of power and signal cables.

Internal Fixed Structure: In Figure 2(b), the motor mounts on the winch winding wheel. The circuit and transmission plates are connected to the bearing's inner ring, rotating relative to the winch via a crossed roller bearing. This design is suitable when the winch is fixed, simplifying wiring by avoiding cable rotation.

2.1.2 Choices for first-stage reduction mechanisms

Pulley Reduction Mechanism: Figure 3(a) shows a belt-driven system where a small motor pulley drives a larger pulley on the winch shaft. Ideal for reduction ratios of 1–2.5, it offers compact size, light weight, and low noise, beneficial in space-constrained designs.

Gear Reduction Mechanism: Figure 3(b) illustrates a gear-based reduction: a pinion on the motor drives a larger gear on the winch shaft. Suitable for ratios above 2.5, it provides high transmission accuracy and load capacity, despite requiring more space.

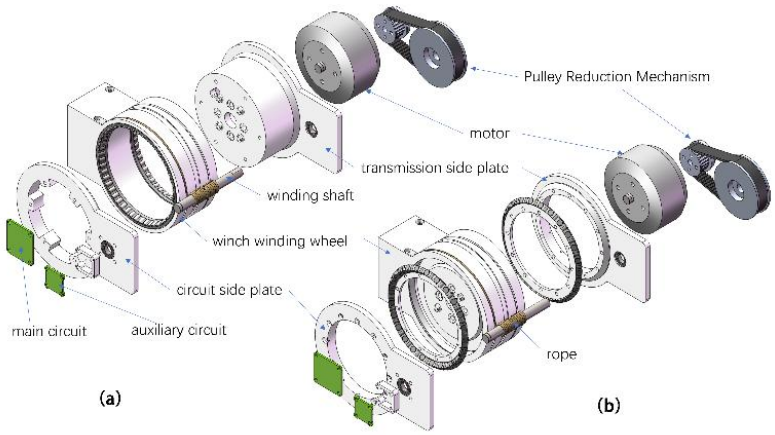

Figure 2 Exploded Views of Motor Mounting Methods: (a) External Fixed; (b) Internal Fixed

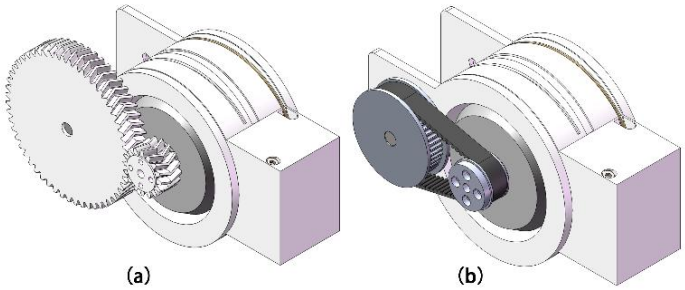

Figure 3 Primary Transmission Methods: (a) Gear-Based; (b) Belt-Based

2.2 Reduction Ratio Calculation

The overall reduction ratio i of the reducer is:

$$i=i_1 \cdot i_2 \tag{1}$$

where i_1 represents the reduction ratio of the first-stage reduction mechanism, and i_2 represents the reduction ratio of the second-stage winch reduction mechanism. The first-stage reduction ratio i_1 is determined by the tooth ratio of the pulley or gear, calculated as:

$$i_1=\frac{z_2}{z_1} \tag{2}$$

where z_1 is the number of teeth on the driving pulley (or gear), and z_2 is the number of teeth on the driven pulley (or gear).The reduction ratio i_2 of the second-stage winch mechanism requires correction based on the diameter of the rope. Due to the tension applied during winding, the cross-sectional shape of the rope undergoes deformation. The corrected reduction ratio i_2 is:

$$i_2=\frac{D_2+\lambda d}{D_1+\lambda d} \tag{3}$$

As shown in Figure 4(a), D_1 is the diameter of the winch winding shaft, D_2 is the diameter of the winch winding wheel, d is the cross-sectional diameter of the rope in a slack state, and λ is the deformation coefficient representing the cross-sectional height change of the rope when under tension. The cross-sectional area of the rope is generally assumed to remain approximately constant after deformation. As shown in Figure 4(b). Based on empirical data, λ is typically selected between 0.6 and 0.9, depending on factors such as the degree of bending of the rope, the tension force, and the properties of the material.

2.3 Dimension Calculation Method

In the second-stage winch reduction mechanism, the winch winding wheel must be designed with grooves to prevent the rope from sliding laterally during joint rotations. Without groove design, the rope overlaps and tangling may occur, potentially causing joint jamming. The groove design effectively eliminates this issue.

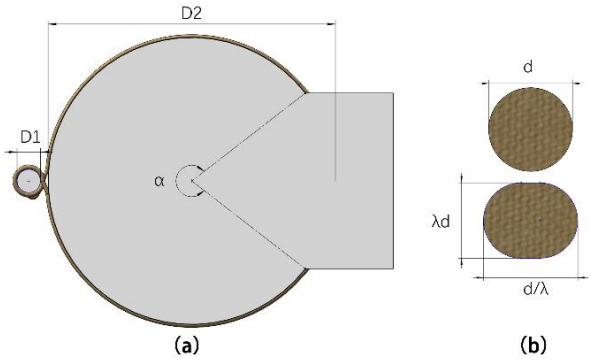

Figure 4 Winding Schematic Diagram

The grooves on the winch winding wheel are divided into two groups. The first group is distributed helically on both sides of the winding wheel. The pitch p of the helical grooves satisfies the following equation:

$$p=\frac{i_2 \cdot d}{\lambda} \tag{4}$$

The cross-sectional height of these grooves is λd, and the width is d/λ.
The second group of grooves is located centrally, with a width of approximately $2d/\lambda$ and a height of λd. These central grooves serve primarily to avoid interference with rope knots, which will be discussed in detail in Section 3.

2.4 Design parameters and specifications

As shown in Table 1, a set of typical design values for a two-stage reduction joint actuator is presented. These values have been experimentally verified and serve as references for the design. The specific measurement process is not elaborated upon in this paper.

Table 1 Joint Basic Data Table

D1	8 mm	Weight	700 g
D2	100 mm	Motor Model	6215
d	1.5 mm	Rated Torque	30 Nm
H	45 mm	Peak Torque	50 Nm
i1	50/23	Backdriving	0.6 Nm
i2	10.9	Rated Power	500 W

3 WINDING AND TENSIONING METHODS

The mechanical structure of rope-driven systems must address the issues of rope fixation and tensioning. This section discusses how proper winding methods can prevent rope slippage and how to apply appropriate tension. Winding methods and testing

In a two-stage winch reduction mechanism, it is crucial to ensure stable output torque and avoid measurement errors in the output shaft angle by preventing relative slippage between the winch winding shaft and the rope. Assuming the rope is wound around the shaft in multiple loops, the Euler friction equation can be used to calculate the critical friction force. When the two-stage winch outputs torque, the tension at both ends of the rope changes according to the following relationship:

$$T_1=\frac{\tau}{D_2/2}+T_2 \tag{5}$$

where T_1 and T_2 represent the tensions at both ends of the rope, and τ is the output torque limited solely by friction. To ensure T_1 and T_2 are greater than zero, pre-tensioning is required. Assuming equal pre-tension T at both ends, we have:

$$T=\frac{T_1+T_2}{2} \tag{6}$$

with $T_1>0$, $T_2>0$. If the rope does not cross itself during winding, as shown in Figure 5(a), the Euler friction equation gives:

$$T_2=e^{\mu\beta}T_1 \tag{7}$$

Here, μ is the static friction coefficient between the rope and the winding shaft, and β is the wrap angle of the rope on the shaft. Combining Equations (1)–(4), the relationship between pre-tension and torque is derived:

$$\frac{T+\frac{\tau}{D_2}}{T-\frac{\tau}{D_2}}=e^{\mu\beta} \tag{8}$$

with $T\geq\frac{\tau}{D_2}$. From these equations, it follows that the pre-tension must be proportional to the output torque to prevent the slippage. However, this design introduces two issues:

Limited Joint Overload Capacity: If the output torque exceeds the set limit, slippage occurs, restricting overload performance.

Rope Creep: Over time, the rope undergoes plastic deformation under sustained tension, reducing the pre-tension T and thus lowering the maximum sustainable torque.

3.1 Improved Knot Method

To address these issues, this paper proposes a novel knot structure. The knot wraps the rope through a central hole on the winding shaft, leveraging the friction between rope segments to prevent slippage, as shown in Figure 5 (b). Experimental results show that when $T_2=0$ and no additional loops are present, the rope does not slip even under a sustained tensile force of over 1000 N at T_1. This suggests a self-locking effect of the knot. In this scenario, Equations (7) and (8) no longer apply, and there is no direct linear relationship between pre-tension and torque. Nevertheless, due to the rope's inherent elasticity, a certain amount of tension is still required to maintain the stable winding.

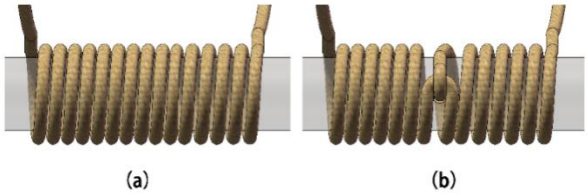

Figure 5 Two Winding Methods

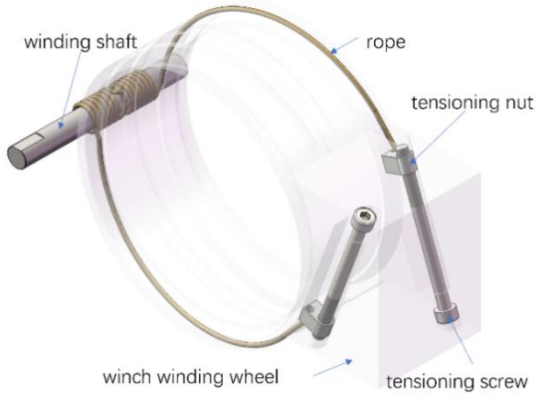

Figure 6 Tension Method

When $T_1>2T$, we have $T_2=0$, indicating slack on one side of the rope. Assuming the rope remains in the groove without lateral displacement and retains its arc shape when slack, the following condition must be satisfied to prevent the rope from leaving the groove:

$$D_2(e-2e')<\frac{d}{2} \tag{9}$$

where e is the elongation ratio of the rope under torque τ, e' is the elongation ratio caused by pre-tension T without torque, and d is the rope diameter. The elongation ratios satisfy:

$$e=\frac{2\tau}{D_2EA},\ e'=\frac{T}{EA} \tag{10}$$

where E is the Young's modulus of the rope, and A is its cross-sectional area. Combining Equations (9)–(10), the required pre-tension T is:

$$T>\frac{\tau}{D_2}-\frac{dEA}{4D_2} \tag{11}$$

Thus, even with the self-locking knot, a certain level of pre-tension is still necessary to keep the rope securely in the groove. Additionally, to accommodate rope creep, increasing the initial pre-tension can provide a margin for deformation.

3.2 Tensioning Method and Testing

To pre-tension the rope, a tensioning system is designed (Figure 6), mounted on the winch wheel. It consists of a guiding groove, a tensioning nut, and a tensioning screw. The groove prevents lateral rope displacement, while the nut secures the rope end and connects to the screw, which applies the tensioning force.

Due to space constraints preventing direct force sensing, the rope tension is estimated by measuring the torque applied to the tensioning screw. This torque balances three forces proportional to the tensile force: thread friction, a component of the screw-nut support force, and friction at the screw head. Given the difficulty in determining friction coefficients, a test under identical conditions was conducted using M4 screws (screw head against PLA). A tensile tester measured rope tension, and a torque screwdriver measured screw torque. Results show an approximately linear relationship, allowing actual tension to be determined from screw torque via the calibration curve.

4 ELECTRONIC CIRCUIT AND DUAL-ENCODER DESIGN

4.1 Electronic Circuit Design

The joint's electronic system comprises a main circuit and an auxiliary circuit (Figure 7). The main circuit, based on an STM32G431 controller, integrates a buck converter, a three-phase inverter for motor driving, and a single-turn absolute encoder measuring the motor shaft's magnet. It communicates externally via RS485 and with the auxiliary circuit via SPI. The auxiliary circuit contains another single-turn absolute encoder to measure the angle of the winch winding shaft.

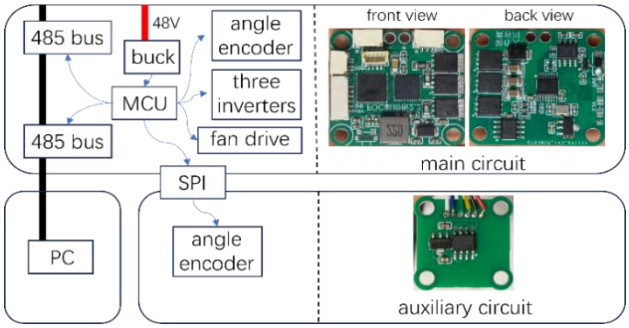

Figure 7 Control Circuit System Structure

4.2 Dual-Encoder Design

The dual-encoder system is designed to ensure that the absolute angle of the output shaft can be determined after the joint motor is powered off and restarted. Instead of directly measuring the output shaft or using additional gears, our method calculates the output angle by combining the measured angles from both the motor and the winch winding shaft. Assuming the motor angle measurement is θ_a, the winch drum angle measurement is θ_b. The multi-turn motor rotation angle is θ, and the reducer rotation angle is θ/i. Then,

$$\theta=\theta_a+360\,k,\quad k\in\mathbb{Z} \tag{12}$$

$$\theta_b=(\theta/i_1)\bmod 360 \tag{13}$$

where k can be regarded as the number of motor revolutions. Substituting (12) into (13) yields:

$$\theta_b=\left(\frac{\theta_a}{i_1}+360\,\frac{k}{i_1}\right)\bmod 360 \tag{14}$$

To uniquely determine k from (θ_a,θ_b), it is required that k has a unique solution for $0\le k<i$. Equation (15) ensures the uniqueness of k, thereby allowing the unique determination of θ and the reducer rotation angle θ/i.

$$i \leq \frac{z_2}{\gcd(z_1, z_2)} \tag{15}$$

5 CONCLUSIONS

Experiments confirm that the proposed module achieves a high effective reduction ratio, predictable output stiffness close to the analytical model, and improved backdrivability at a comparable size and mass. The dual-encoder system reliably resolves the output shaft's absolute position after power cycling, enabling precise robotic control.
Future work includes strength limit testing to study failure modes and long-term operation tests for fatigue and wear analysis. The joint module can be applied to legged robots like quadrupeds or humanoids to improve lightweight performance and impact tolerance.

COMPETING INTERESTS

The authors have no relevant financial or non-financial interests to disclose.

REFERENCES

[1] Patrick Wensing M, Benjamin Katz B, et al. Dynamic Locomotion in the MIT Cheetah 3 Through Convex Model-Predictive Control. 2018 IEEE/RSJ International Conference on Intelligent Robots and Systems (IROS), 2018: 1-9.
[2] Malik A A, Masood T, Brem A. Intelligent humanoids in manufacturing to address worker shortage and skill gaps: Case of Tesla Optimus. arXiv preprint arXiv:2304.04949, 2023. https://arxiv.org/abs/2304.04949.
[3] Lickindorf D. Stanley - the Capstan Based Quadruped Kit. Hackaday, 2025. https://hackaday.io/project/181769-stanley-the-capstanbased-quadruped-kit.
[4] Negrello F, Garabini M, Catalano MG, et al. A modular compliant actuator for emerging high performance and fall-resilient humanoids. 2015 IEEE-RAS 15th International Conference on Humanoid Robots (Humanoids), 2015: 414-420.
[5] Song H, Kim YS, Yoonet J, al. Development of Low-Inertia High Stiffness Manipulator LIMS2 for High-Speed Manipulation of Foldable Objects. 2018 IEEE/RSJ International Conference on Intelligent Robots and Systems (IROS), 2018: 4145-4151.
[6] Tanaka K, Hamaya M. Twist Snake: Plastic table-top cable-driven robotic arm with all motors located at the base link. 2023 IEEE International Conference on Robotics and Automation (ICRA), 2023: 7345-7351.
[7] Wang Z, Freris N M, Wei X. SpiRobs: Logarithmic spiral-shaped robots for versatile grasping across scales. Device, 2025, 3(4): 100646. DOI: 10.1016/j.device.2024.100646.
[8] Li F, Yang H, Gu G, et al. Position and Orientation Tracking Control of a Cable-Driven Tensegrity Continuum Robot. IEEE Transactions on Robotics, 2025, 41: 1791-1811. DOI: 10.1109/TRO.2025.3543292.